eLIFE
elifesciences.org

RESEARCH ARTICLE

The conserved aspartate ring of MCU mediates MICU1 binding and regulation in the mitochondrial calcium uniporter complex

Charles B Phillips[1], Chen-Wei Tsai[1,2], Ming-Feng Tsai[1,2]*

[1]Department of Biochemistry, Brandeis University, Waltham, United States; [2]Department of Physiology and Biophysics, University of Colorado Anschutz Medical Campus, Aurora, United States

Abstract The mitochondrial calcium uniporter is a Ca^{2+} channel that regulates intracellular Ca^{2+} signaling, oxidative phosphorylation, and apoptosis. It contains the pore-forming MCU protein, which possesses a DIME sequence thought to form a Ca^{2+} selectivity filter, and also regulatory EMRE, MICU1, and MICU2 subunits. To properly carry out physiological functions, the uniporter must stay closed in resting conditions, becoming open only when stimulated by intracellular Ca^{2+} signals. This Ca^{2+}-dependent activation, known to be mediated by MICU subunits, is not well understood. Here, we demonstrate that the DIME-aspartate mediates a Ca^{2+}-modulated electrostatic interaction with MICU1, forming an MICU1 contact interface with a nearby Ser residue at the cytoplasmic entrance of the MCU pore. A mutagenesis screen of MICU1 identifies two highly-conserved Arg residues that might contact the DIME-Asp. Perturbing MCU-MICU1 interactions elicits unregulated, constitutive Ca^{2+} flux into mitochondria. These results indicate that MICU1 confers Ca^{2+}-dependent gating of the uniporter by blocking/unblocking MCU.
DOI: https://doi.org/10.7554/eLife.41112.001

***For correspondence:** ming-feng.tsai@ucdenver.edu

Competing interests: The authors declare that no competing interests exist.

Funding: See page 13

Received: 14 August 2018
Accepted: 07 January 2019
Published: 15 January 2019

Reviewing editor: Baron Chanda, University of Wisconsin-Madison, United States

Introduction

The mitochondrial calcium uniporter is a multi-subunit Ca^{2+}-activated Ca^{2+} channel complex located in the inner mitochondrial membrane (IMM). It catalyzes Ca^{2+} influx from the intermembrane space (IMS) into the mitochondrial matrix, where a large quantity of Ca^{2+} can be stored. Extensive studies have established that the uniporter regulates spatial and temporal dimensions of intracellular Ca^{2+} signals, as well as Ca^{2+}-dependent mitochondrial processes, including oxidative phosphorylation and programmed cell death (***Kamer and Mootha, 2015***; ***Rizzuto et al., 2012***).

The Ca^{2+}-conducting function of mammalian uniporters are mediated by two subunits, MCU and EMRE, in the transmembrane (TM) region (***Figure 1***). The MCU protein possesses two TM helices and a highly-conserved 'DIME' signature sequence (***Baughman et al., 2011***; ***De Stefani et al., 2011***). High-resolution structures (***Baradaran et al., 2018***; ***Fan et al., 2018***; ***Nguyen et al., 2018***; ***Yoo et al., 2018***) show that MCU assembles into a tetrameric Ca^{2+} pore, with the DIME-Asp and -Glu forming two parallel side-chain carboxylate rings to constitute a Ca^{2+} selectivity filter at the pore's IMS entrance (***Figure 1***). The single-pass EMRE protein binds to MCU via its TM helix (***Tsai et al., 2016***). This interaction is shown to be necessary for Ca^{2+} permeation (***Tsai et al., 2016***; ***Kovács-Bogdán et al., 2014***; ***Sancak et al., 2013***).

The uniporter is tightly regulated by intracellular Ca^{2+} signals. It stays quiescent in resting cellular conditions, and becomes activated only when IMS Ca^{2+} increases to low micromolar levels (***Csordás et al., 2013***; ***Mallilankaraman et al., 2012***). This Ca^{2+}-dependent gating is mediated by

two EF-hand (a helix-loop-helix Ca^{2+}-coordinating motif) containing subunits: MICU1 and MICU2 (the neuron-specific MICU3 is not discussed here) (**Csordás et al., 2013**; **Mallilankaraman et al., 2012**; **Perocchi et al., 2010**; **Plovanich et al., 2013**), which are tethered to the uniporter's TM region via the C-terminal tail of EMRE (**Tsai et al., 2016**). Depletion of MICU1 eliminates Ca^{2+}-regulation of the uniporter, causing the channel to constitutively load Ca^{2+} into the matrix (**Tsai et al., 2016**; **Mallilankaraman et al., 2012**; **Plovanich et al., 2013**; **Tsai et al., 2017**), a condition linked to debilitating neuromuscular disorders in humans (**Logan et al., 2014**). Currently, the mechanism by which MICUs control Ca^{2+} transport via MCU remains largely unknown.

Here, we demonstrate that MICU1 interacts with MCU's DIME-Asp via a Ca^{2+}-modulated electrostatic interaction. This is mediated by two closely-spaced Arg residues on the surface of MICU1. MICU2, which lacks these Args, does not bind MCU. Mutations that disrupt the MCU-MICU1 interaction severely perturbs Ca^{2+}-regulation of the uniporter. These results led to a molecular mechanism in which MICUs open or close the uniporter in response to intracellular Ca^{2+} signals by physically blocking or unblocking the MCU pore.

Results

Evolutionarily conserved MCU-MICU1 interactions

Phylogenetic analyses (**Sancak et al., 2013**; **Bick et al., 2012**) have shown that uniporters in lower eukaryotes (*e.g.*, plants and protists) contain only MCU and MICU1 subunits, raising a possibility that MICU1 might gate MCU via direct molecular contacts. If so, these interactions might be conserved in evolution to ensure proper regulation of the uniporter. To test this idea, we performed co-immunoprecipitation (CoIP) experiments to examine complex formation between human MICU1 and various MCU homologues in MCU/EMRE-KO HEK 293 cells (**Tsai et al., 2016**). The EMRE gene is deleted because EMRE can bind both MCU and MICU1 (**Figure 1**) (**Tsai et al., 2016**; **Sancak et al., 2013**), and would therefore complicate assessment of direct MCU-MICU1 contacts. **Figure 2** shows that human MICU1 pulls down not only human MCU but also MCU homologues in *D. melanogaster*, *C. elegans*, *D. discoideum*, and *A. thaliana,* indicating that the MCU-MICU1 interaction is indeed evolutionarily conserved.

The role of the DIME-Asp in Ca^{2+} transport and MICU1 binding

We reasoned that MICU1 might bind to the DIME-Asp, as MCU structures (**Baradaran et al., 2018**; **Fan et al., 2018**; **Nguyen et al., 2018**; **Yoo et al., 2018**) show that this Asp is the only fully-conserved residue with the side-chain exposed to the IMS, where MICU1 is localized. Accordingly, the DIME-Asp in human MCU was mutated to Ala (D261A), and the mutant was expressed in MCU-KO HEK 293 cells for analysis. Surprisingly, a standard mitochondrial Ca^{2+} uptake assay shows that D261A MCU is capable of importing Ca^{2+} (10 μM), with the rate of transport unaffected by adding 100 mM Na^{+}, which has an ionic radius virtually identical to Ca^{2+} (**Figure 3** and **Figure 3—figure supplement 1**). A quantitative $^{45}Ca^{2+}$ flux experiment (**Tsai et al., 2016**) performed in 10 μM Ca^{2+} shows that D261A slows MCU's Ca^{2+} transport by only 3.8-fold (**Figure 3—figure supplement 2**), an effect remarkably small considering the critical position of this residue in the pore (**Baradaran et al., 2018**; **Fan et al., 2018**; **Nguyen et al., 2018**; **Yoo et al., 2018**). In contrast, mutating the DIME-Glu (E264) to Ala, Asn, or Gln abolishes uniporter function (**Figure 3** and **Figure 3—figure supplements 2** and **3**), as expected from its key role in coordinating Ca^{2+} in the selectivity filter (**Baradaran et al., 2018**; **Fan et al., 2018**; **Nguyen et al., 2018**; **Yoo et al., 2018**). To further pursue these observations, D261 was mutated to all other 18 amino-acids. Only D, E and A at this position support Ca^{2+} transport (**Figure 3—figure supplement 3**).

We then performed CoIP to test how wild-type (WT) MICU1 binding responds to MCU mutations at D261 and E264. Results show that MICU1 binds WT, D261E, and E264A MCU, but not D261A or D261Q (**Figure 4**). Although the D261Q mutant cannot transport Ca^{2+}, it still assembles as oligomers (**Figure 4—figure supplement 1**), suggesting that the mutation does not compromise MCU's structural integrity. These results demonstrate that the DIME-Asp mediates MCU interaction with MICU1, instead of contributing essentially to Ca^{2+} permeation.

It was observed that D261A loses sensitivity to a potent and specific uniporter inhibitor Ru360 (**Matlib et al., 1998**),20 (**Figure 3B**). This is consistent with the thought that D261 contributes to a

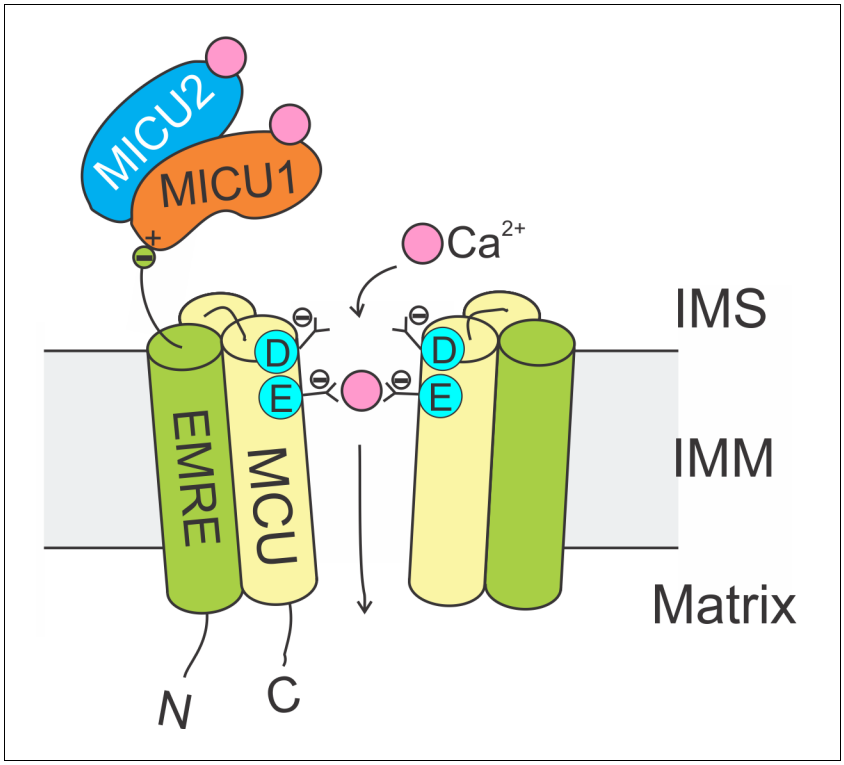

Figure 1. Molecular assembly of the mitochondrial Ca^{2+} uniporter. The MCU protein assembles into a tetrameric Ca^{2+} pathway across the inner mitochondrial membrane (only two subunits are illustrated to reveal the Ca^{2+} pore). Conserved Asp and Glu residues in MCU's DIME signature sequence form two parallel side-chain carboxylate rings at the IMS entrance of the pore to coordinate Ca^{2+}. The EMRE protein binds to MCU and MICU1 via its TM helix and C-terminal tail, respectively. When an intracellular Ca^{2+} signal arrives at the IMS surface of the uniporter, Ca^{2+} binding to MICUs leads to activation of the uniporter to transport Ca^{2+} into the matrix.
DOI: https://doi.org/10.7554/eLife.41112.002

Ru360 site in MCU (***Arduino et al., 2017***; ***Cao et al., 2017***), and implies that MICU1 and Ru360 inhibitory sites overlap. A previous study shows that the S259A mutation diminishes Ru360 inhibition (***Baughman et al., 2011***), raising a possibility that S259 might also be involved in MICU1 binding. We confirm that S259A reduces Ru360 inhibition of the uniporter by 82 ± 3% (***Figure 4—figure supplement 2***), and show that this mutation indeed destabilizes the MCU-MICU1 complex (***Figure 4—figure supplement 2***), albeit to a lesser degree than D261A. It thus appears that MCU and MICU1 form a multi-residue contact surface containing S259 and D261 in MCU, with the latter playing a more critical role in mediating tight MCU-MICU1 interactions.

Electrostatic interactions between MCU and MICU1

As DIME-Asp appears as a fourfold ring of negative charges facing the IMS, it is tempting to picture MICU1 as a classic pore-blocker (***Banerjee et al., 2013***; ***Park and Miller, 1992***) electrostatically stabilized on MCU's ion entryway. This picture is strongly supported by the observation that the MCU-MICU1 interaction can be weakened or strengthened by raising or lowering ionic strength, respectively (***Figure 5A***). In contrast, neither dissociation of the MICU1-MICU2 dimer nor the 1D4-tag and anti-1D4 antibody epitope interaction is affected by varying ionic strength (***Figure 5—figure supplement 1***). To search MICU1 for electrostatic binding partners of the DIME-Asp, we launched an Ala mutagenesis screen targeting 18 conserved Arg or Lys residues in human MICU1 (***Figure 5—figure supplement 2***). Only R119 and R154, two residues closely spaced on the protein's surface (***Wang et al., 2014***), were found to abolish MCU binding upon mutation to Ala (***Figure 5B*** and ***Figure 5—figure supplement 3***). These mutants, like WT MICU1, form heterodimers with MICU2 (***Patron et al., 2014***) (***Figure 5—figure supplement 4***), indicating proper protein folding. Moreover,

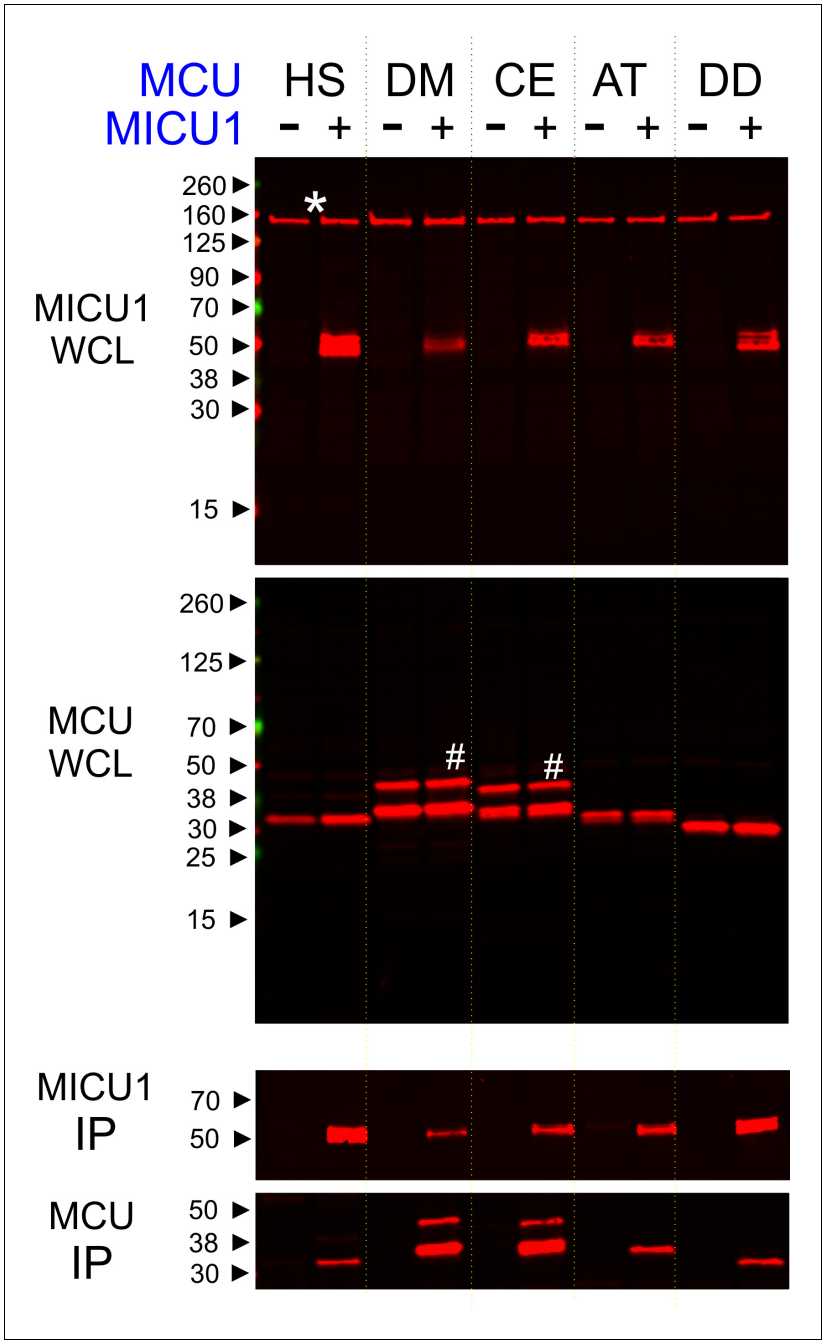

Figure 2. Conserved MCU-MICU1 interactions. 1D4-tagged MCU homologues from various species (HS: *Homo sapiens*, DM: *Drosophila Melanogaster*, CE: *Caenorhabditis elegans*, AT: *Arabidopsis thaliana*, and DD: *Dictyostelium discoideum*) were expressed in the presence or absence of FLAG-tagged WT human MICU1 in MCU/EMRE-KO cells. MICU1 was immobilized in FLAG-affinity resins to pull down MCU. Anti-FLAG and anti-1D4 antibodies were used to detect MICU1 and MCU, respectively. SDS-PAGE was performed under reducing conditions. *WCL*: whole cell lysate. *IP*: immunoprecipitation. *Asterisk*: non-specific Western signals. *Hash*: MCU homologues that contain untruncated mitochondrial-targeting sequences.
DOI: https://doi.org/10.7554/eLife.41112.003

R119K or R154K mutants remain associated with MCU, while Glu or Gln substitutions in these two positions strongly disrupt MCU binding (***Figure 5—figure supplement 5***). Neither of the two Arg residues is present in MICU2, and MICU2 is indeed unable to complex with MCU (***Figure 5C***). Taken

together, the data suggest that R119 and R154 in MICU1 mediate electrostatic interactions with the DIME-Asp in MCU.

Functional roles of the MCU-MICU1 interaction

We have thus far utilized transiently expressed WT or mutant MICU1 to identify molecular determinants of the MCU-MICU1 interaction. However, as MICU1 exclusively forms a disulfide-connected heterodimer with MICU2 in mammalian cells (***Patron et al., 2014***; ***Petrungaro et al., 2015***), it is necessary to exclude the possibility that dimerization with MICU2 could fundamentally alter how MICU1 contacts MCU. Accordingly, we employed MCU to pull down native MICUs. Results show that the D261A mutation disrupts MCU association with the physiological MICU1-2 heterodimer (***Figure 6***), indicating that the MICU2-bound form of MICU1 still interacts with MCU via the DIME-Asp.

As binding of MICU1 to the DIME-Asp would likely block the uniporter's pore, we hypothesize that MICU1 shuts the uniporter in resting Ca^{2+} (<1 μM) through this particular interaction. This hypothesis predicts that (1) raising Ca^{2+} to micromolar levels would disrupt MCU's association with the MICU1-2 heterodimer, and that (2) perturbing the MCU-MICU1 interaction by mutating the DIME-Asp or R119/R154 would prevent MICU1 from shutting the uniporter. Indeed, CoIP experiments show that supplying 10 μM Ca^{2+} breaks the MCU-MICU1-MICU2 complex (***Figure 6***). The $^{45}Ca^{2+}$ flux assay described above was subsequently used to quantify mitochondrial uptake under a low Ca^{2+} (0.5 μM) condition. In WT cells, little Ca^{2+} entry (1.6 ± 0.9 pmol/min/10^6 cells) into mitochondria was detected (***Figure 7A***). As expected, MICU1-KO induces robust Ca^{2+} influx (205 ± 11

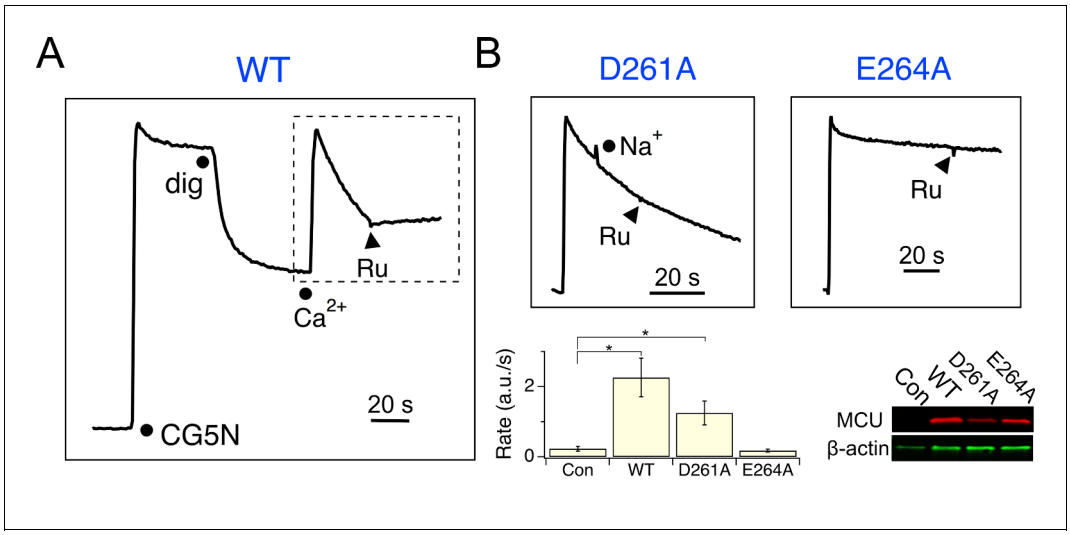

Figure 3. Functional analysis of MCU. (**A**) A fluorescence-based mitochondrial Ca^{2+} uptake assay. MCU-KO HEK293 cells, transiently expressing WT MCU, were permeabilized with digitonin (dig) in the presence of an extracellular Ca^{2+} indicator Calcium Green-5N (CG5N). Adding 10 μM $CaCl_2$ leads to an immediate increase of fluorescence, followed by a signal decline reflecting uniporter-mediated Ca^{2+} uptake. Ru360 (Ru) was added to inhibit the channel. In subsequent experiments, only traces obtained after applying Ca^{2+} (dashed box) are presented. (**B**) The activity of D261A or E264A mutants. These mutants were expressed in MCU-KO cells, with 100 mM NaCl added during Ca^{2+} uptake to test if the channel can select Ca^{2+} against Na^+. The bar chart summarizes the initial rate of Ca^{2+} uptake, and the western blot compares expression levels of MCU constructs. *Con*: untransfected cells. *p<0.01.

DOI: https://doi.org/10.7554/eLife.41112.004

The following figure supplements are available for figure 3:

Figure supplement 1. The response of WT MCU to Na^+.

DOI: https://doi.org/10.7554/eLife.41112.005

Figure supplement 2. Quantification of uniporter Ca^{2+} transport.

DOI: https://doi.org/10.7554/eLife.41112.006

Figure supplement 3. The activity of D261 or E264 MCU mutants.

DOI: https://doi.org/10.7554/eLife.41112.007

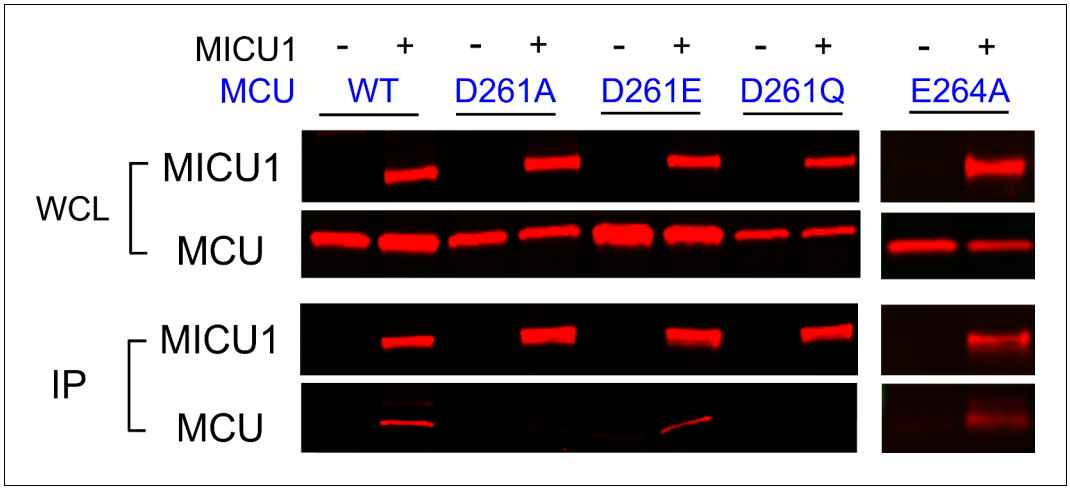

Figure 4. The impact of D261 or E264 mutations on MICU1 binding. FLAG-tagged WT MICU1 was used to pull down various MCU mutants co-expressed in MCU/EMRE-KO cells.

DOI: https://doi.org/10.7554/eLife.41112.008

The following figure supplements are available for figure 4:

Figure supplement 1. Oligomerization of D261 mutants.

DOI: https://doi.org/10.7554/eLife.41112.009

Figure supplement 2. The role of S259 in Ru360 inhibition and MICU1 binding.

DOI: https://doi.org/10.7554/eLife.41112.010

pmol/min/10^6 cells), a phenotype partially reversed by expressing WT MICU1 (53 ± 4 pmol/min/10^6 cells, ***Figure 7A***). We then introduced WT or D261A MCU into MCU-KO cells. In low Ca^{2+}, WT MCU exhibits no activity (1.7 ± 0.5 pmol/min/10^6 cells) while D261A mediates a Ca^{2+} influx (34 ± 5 pmol/min/10^6 cells) 6.2-fold slower than that observed in MICU1-KO cells (***Figure 7B***). A few factors might underlie the rather small magnitude of the D261A-mediated Ca^{2+} uptake: (1) this mutant is 3.8-fold slower than WT MCU (***Figure 3—figure supplement 2***), (2) our transfection efficiency is ~80%, and (3) other residues (e.g., S259) are also involved in MICU1 binding. A S259A/D261A double mutant was constructed to further disrupt the MCU-MICU1 interface, but unfortunately its function could not be analyzed due to a low expression level (***Figure 4—figure supplement 2***). The finding that D261A catalyzes unregulated Ca^{2+} flux in submicromolar Ca^{2+} argues strongly that MICU1 must contact MCU to gate the uniporter. Lastly, we tested R119 or R154 mutants in MICU1-KO cells. All of these, except for R154Q, are less competent than WT MICU1 in restoring Ca^{2+} regulation of the uniporter (***Figure 7C***), a result confirming the critical role of the MCU-MICU1 interaction in Ca^{2+}-activation of the uniporter.

Discussion

The mitochondrial Ca^{2+} uniporter plays a crucial physiological role of regulating cytoplasmic Ca^{2+} signals and controlling mitochondrial metabolic and apoptotic pathways. These processes require the uniporter to remain strictly quiescent in resting cellular conditions. Here, we propose a mechanism (***Figure 8***) in which MICU1 shuts the uniporter by binding to the DIME-Asp side-chain carboxylate ring to block the IMS entrance of the MCU pore. Upon arrival of intracellular Ca^{2+} signals, Ca^{2+} binding to MICU1 at its EF hands disrupts this interaction, thus leading to opening of this Ca^{2+}-activated Ca^{2+} channel.

The EMRE subunit, which binds both MCU and MICU1 (***Tsai et al., 2016***), plays an important role in this mechanism. It has been shown that the EMRE-MICU1 interaction is necessary to prevent MICU1 dissociation from the uniporter complex (***Tsai et al., 2016***). We can now understand this observation in light of new results here: When MCU and MICU1 separate due to Ca^{2+} elevation, EMRE's tether to MICU1 would prevent this subunit from dissociating away. Thus, once the Ca^{2+} signal is over, MICU1 could rapidly bind to MCU to terminate Ca^{2+} influx (***Figure 8***).

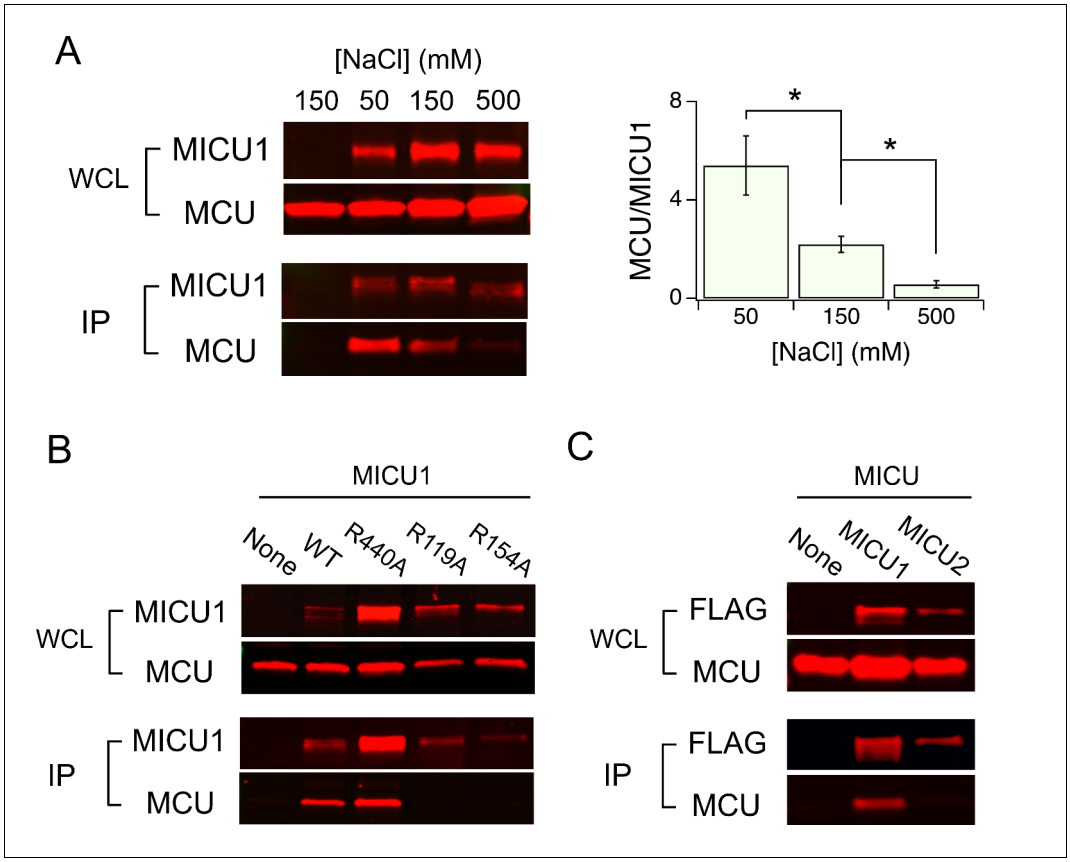

Figure 5. Electrostatic interactions between MCU and MICU1. (**A**) Modulation of MCU-MICU1 complex stability by ionic strength. WT MCU and MICU1 were expressed in MCU/EMRE-KO cells, and CoIP experiments were performed in the presence of 50, 150, or 500 mM of NaCl. The IP signal of MCU was normalized to that of MICU1, with the ratio presented in the bar chart. (**B**) The effect of MICU1 Arg mutations on MCU binding. (**C**) A CoIP experiment testing if MCU and MICU2 form complexes. MICU2 was FLAG-tagged to precipitate WT MCU in MCU/EMRE-KO cells. *p<0.05.

DOI: https://doi.org/10.7554/eLife.41112.011

The following figure supplements are available for figure 5:

Figure supplement 1. The effect of varying ionic strength on protein-protein interactions.

DOI: https://doi.org/10.7554/eLife.41112.012

Figure supplement 2. Multiple sequence alignment of MICU1.

DOI: https://doi.org/10.7554/eLife.41112.013

Figure supplement 3. MICU1 mutagenesis screen.

DOI: https://doi.org/10.7554/eLife.41112.014

Figure supplement 4. MICU1-MICU2 Interactions.

DOI: https://doi.org/10.7554/eLife.41112.015

Figure supplement 5. The effect of R119/R154 mutations on MCU-MICU1 complex formation.

DOI: https://doi.org/10.7554/eLife.41112.016

In this model, MICU2 does not directly contact MCU to block the channel (***Figure 8***). This is consistent with previous work (***Payne et al., 2017***) (but *c.f.* other references, ***Plovanich et al., 2013***; ***Kamer et al., 2017***) showing that MICU2 is not required to gate the uniporter closed. A fundamental issue for the future would be to determine the function of MICU2 (***Payne et al., 2017***). MICU2 likely plays non-redundant roles, as MICUs are present exclusively in the form of MICU1-2 heterodimers in mammalian cells (***Patron et al., 2014***; ***Petrungaro et al., 2015***), and as MICU2 depletion induces severe neuronal and cardiac pathologies (***Bick et al., 2017***; ***Shamseldin et al., 2017***).

During the revision of this manuscript, Paillard *et al.* published an article (***Paillard et al., 2018***) showing that depletion of MICU1 sensitizes the uniporter to Ru360 inhibition. The interpretation was

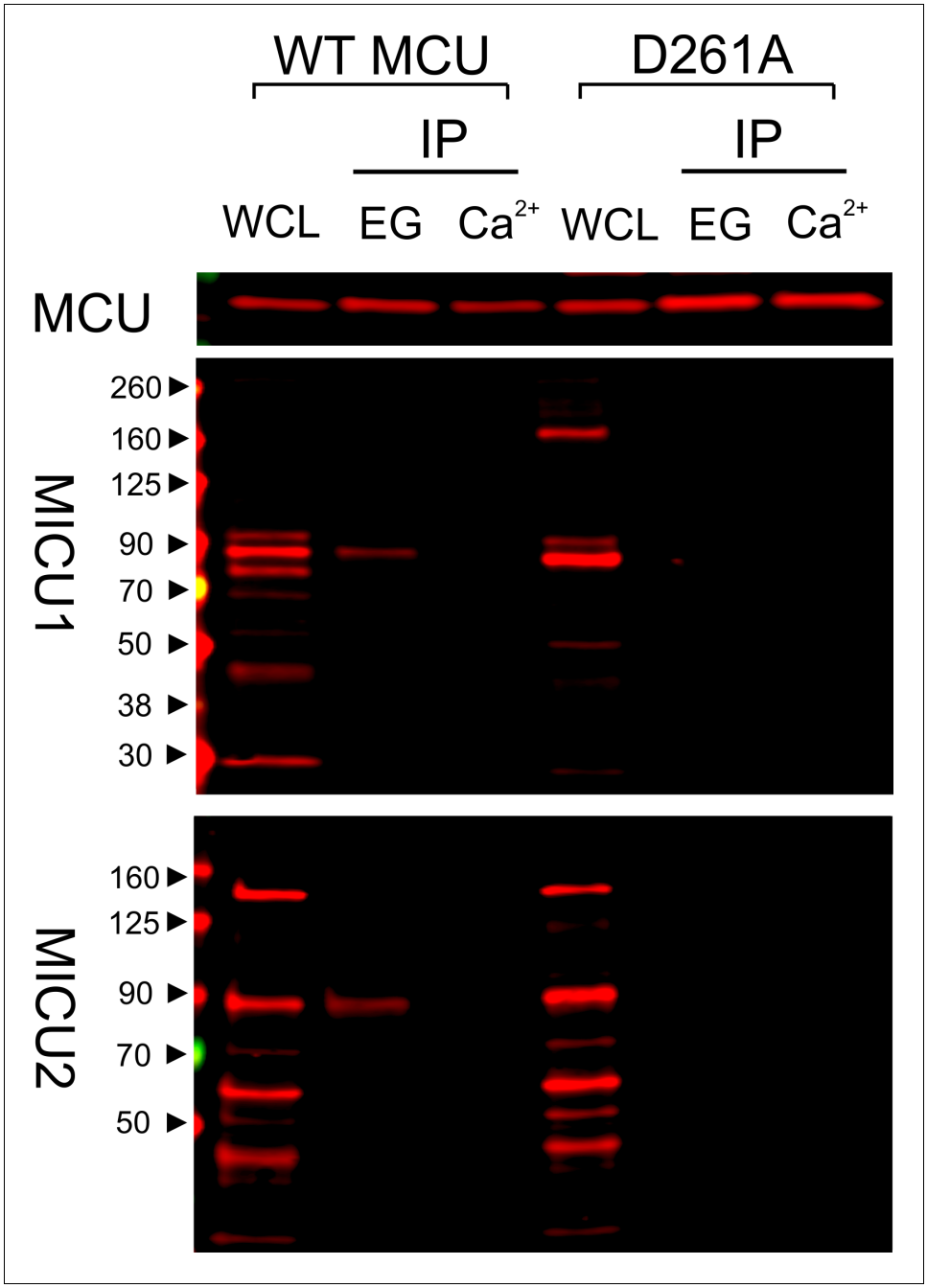

Figure 6. Ca^{2+}-dependent interaction between MCU and the MICU1-2 heterodimer. 1D4-tagged WT or D261A MCU was expressed in WT HEK cells. The cell lysate, after a portion was taken for whole-cell lysate (WCL) analysis, was split into two for CoIP under Ca^{2+}-free (EG, 1 mM EGTA) or 10 μM Ca^{2+} conditions. MCU was used to pull down the native, disulfide-connected MICU1-2 heterodimer (***Patron et al., 2014***; ***Petrungaro et al., 2015***), which has a molecular weight of ~90 kDa. SDS-PAGE was performed in non-reducing environments. MICU1 and MICU2 were detected using anti-MICU1 and -MICU2 antibodies, respectively. WCL signals of MICU1 and MICU2 are not as clean as in previous images (*e.g.*, ***Figure 2***) due to the low abundance of native MICUs and lower qualities of these polyclonal MICU1 and MICU2 antibodies.

DOI: https://doi.org/10.7554/eLife.41112.017

that MICU1 competes for the Ru360 inhibitory site, known to be formed by the DIME-Asp (***Arduino et al., 2017***; ***Cao et al., 2017***). It follows that MICU1 must control the uniporter by interacting with the Asp ring. Our results similarly indicate that MICU1 and Ru360 sites in MCU likely

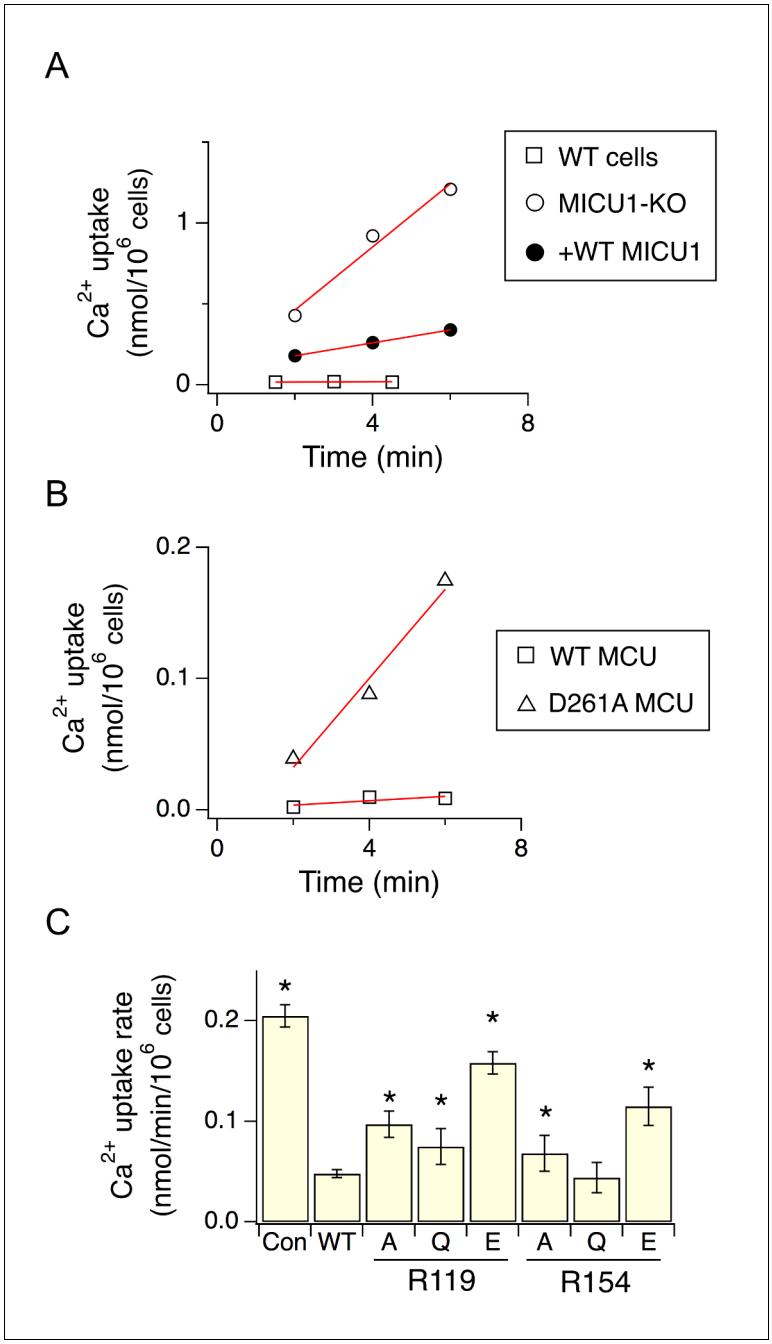

Figure 7. The effect of D261 or R119/R154 mutations on the regulatory function of MICU1. (**A**) Mitochondrial Ca^{2+} uptake in a low Ca^{2+} (0.5 μM) condition. Each data point represents a measurement of $^{45}Ca^{2+}$ transported into mitochondria by the uniporter at a specific time point. These data points were fit with a linear function (red lines) to obtain the rate of Ca^{2+} transport. (**B**) The activity of WT or D261A MCU in 0.5 μM Ca^{2+}. (**C**) A bar chart summarizing the rate of mitochondrial Ca^{2+} uptake. WT MICU1 or various R119/R154 mutants were expressed in MICU1-KO cells. *Con*: untransfected control. Paired t-test was performed between WT MICU1 and mutants. *p<0.05.

DOI: https://doi.org/10.7554/eLife.41112.018

The following figure supplement is available for figure 7:

Figure supplement 1. Data processing in $^{45}Ca^{2+}$flux experiments.

DOI: https://doi.org/10.7554/eLife.41112.019

overlap, as mutations in DIME-Asp and a nearby Ser (S259 in human MCU) perturb both Ru360 inhibition and MICU1 binding.

Paillard *et al.* further proposed that MICU1 uses a DIME-interacting domain (DID) that contains one Lys and two Args (K438, R440, and R443 in human MICU1) to bind MCU. However, it was also shown that with all these residues mutated to Ala, a portion of the MCU-MICU1 complex (~30% of that observed using WT MICU1) remains associated after tens of minutes of incubation in CoIP experiments. This result, which agrees with our finding that R440A or R443A MICU1 forms stable complexes with MCU (***Figure 5—figure supplement 3***), raises a possibility that the DID sequence might not play direct roles in mediating tight MCU-MICU1 interactions.

Our model instead posits that MICU1 uses two closely-spaced Arg in the N-terminal domain (***Wang et al., 2014***) (R119 and R154 in human MICU1) to bind the DIME-Asp (***Figure 8***). This picture is supported by the observations that, consistent with electrostatic interactions, the stability of the MCU-MICU1 complex can be modulated by varying the ionic strength, and that MICU2, which lacks these Args, is unable to bind MCU (the DID sequence is present in both MICU1 and MICU2). The crucial roles of these two Args in MCU binding are further highlighted by the fact that they are the only two basic residues that are conserved in MICU1 homologues in animals, plants, and protists (***Figure 5—figure supplement 2***), in which MCU and MICU1 co-evolve (***Bick et al., 2012***). However, we hasten to point out that, despite these observations, future biochemical and structural work is still required to determine the detailed chemistry that governs MICU1 interactions with the DIME-Asp.

It is known that the uniporter uses a classical multi-ion pore mechanism (***Kirichok et al., 2004***; ***Almers et al., 1984***; ***Hess and Tsien, 1984***) to select Ca^{2+} against >1000-fold more abundant cations such as Na^{+}. In this mechanism, Ca^{2+} binding to a high-affinity site blocks permeation of other cations, while entry of a second Ca^{2+} knocks off the bound Ca^{2+} through electrostatic repulsion to enable high Ca^{2+} flux. New structures of MCU led to the hypothesis that the DIME-Glu forms the high-affinity site (S2) to coordinate a dehydrated Ca^{2+}, while the DIME-Asp forms a second, low-affinity Ca^{2+} site (S1) (***Baradaran et al., 2018***; ***Fan et al., 2018***; ***Nguyen et al., 2018***; ***Yoo et al., 2018***). We systematically mutated DIME-Asp (D261) in human MCU and found that most mutations abolish channel function, an outcome not unexpected considering the critical position of D261 in the pore. The fact that D261A exhibits a comparable activity as WT, however, raises a possibility that other Ca^{2+} sites might be present in proximity to S2 to mediate the electrostatic repulsion required for high Ca^{2+} throughput of the uniporter.

In conclusion, the current study provides a working model to understand how intracellular Ca^{2+} signals control the activity of the uniporter in the molecular level. Major challenges still lie ahead,

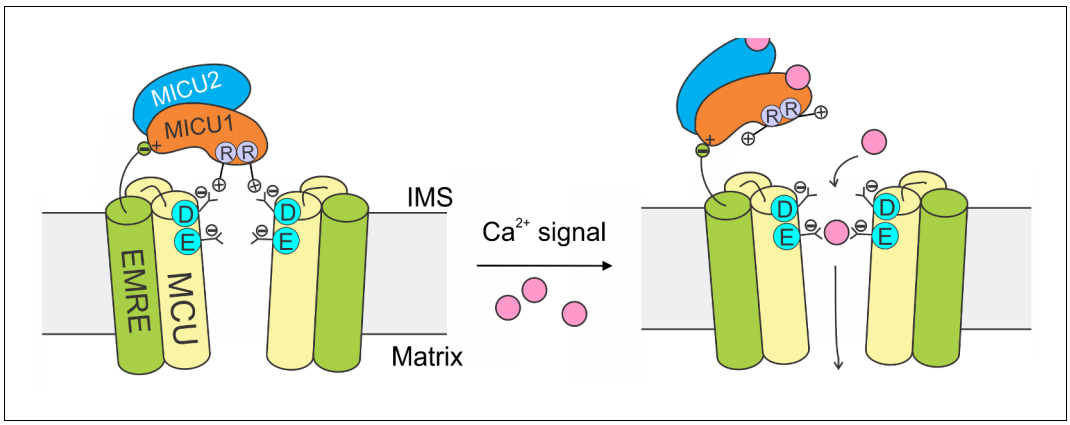

Figure 8. A model of Ca^{2+}-dependent gating of the uniporter. In resting cellular conditions, MICU1 shuts the uniporter by inserting Arg fingers into MCU's Asp ring to occlude the pore. Ca^{2+} activates the channel by binding to MICUs to disrupt this MCU-MICU1 interaction. MICU2 forms a heterodimer with MICU1, but does not directly contact MCU. EMRE plays dual functional roles: it binds to MCU to enable Ca^{2+} permeation, and also interacts with MICU1 to maintain tight association of the MICU1-2 heterodimer with the uniporter during Ca^{2+} stimulation.
DOI: https://doi.org/10.7554/eLife.41112.020

including to understand MICU2's physiological role, to determine how Ca^{2+} disrupts the MCU-MICU1 interaction, and to examine the individual roles of MICU1's two EF hands in channel activation. New electrophysiological and structural tools (**Baradaran et al., 2018**; **Fan et al., 2018**; **Nguyen et al., 2018**; **Yoo et al., 2018**; **Tsai and Tsai, 2018**) will open exciting opportunities to address these in the future.

Materials and methods

Key resources table

Reagent type or resource	Designation	Source or reference	Identifiers	Additional information
Cell line	HEK 293T	ATCC	Cat # CRL-3216	
Cell line	MCU-KO HEK 293T	PMID:27099988		
Cell line	MCU/EMRE-KO HEK 293T	PMID:27099988		
Cell line	MICU1-KO	PMID:28396416		
Primary Antibody	Mouse anti-FLAG	Sigma-Aldrich	Cat # F1804	Western 1:10000
Primary Antibody	Mouse anti-V5	ThermoFisher	Cat # R960-25	Western 1:5000
Primary Antibody	Mouse anti-β actin	Santa Cruz	Cat # 69879	Western 1:500
Primary Antibody	Rabbit anti-MICU1	Sigma-Aldrich	Cat # HPA037480	Western 1:5000
Primary Antibody	Rabbit anti-EFHA1 (MICU2)	Abcam	Cat # ab101465	Western 1:10000
Primary Antibody	Mouse anti-1D4	PMID:6529569		Western 50 ng/mL
Primary Antibody	Mouse anti-C8	PMID:8068416		Western 50 ng/mL
Secondary Antibody	IRDye 680RD goat anti-rabbit IgG	Li-Cor	Cat # 925–68073	Western 1:10000
Secondary Antibody	IRDye 680RD goat anti-mouse IgG	Li-Cor	Cat # 925–68072	Western 1:15000
Chemical compound	Ru360	PMID:2036363		
Chemical compound	$^{45}CaCl_2$	PerkinElmer	Cat # NEX01300	
Commercial kit	Lipofectamine 3000	ThermoFisher	Cat # L3000015	
Commercial kit	Anti-FLAG M2 affinity gel	Sigma-Aldrich	Cat # A2220	
Commercial kit	CNBr-activated Sepharose 4B	GE Healthcare	Cat # 17043001	
Software	Igor Pro 7	WaveMetrics		Figure production and data fitting
Software	ImageStudio 5	Li-Cor		Western-blot quantification
Software	Clustal Omega	PMID:21988835		Sequence alignment
Software	Excel (office 365)	Microsoft		t-test

Reagents, cell culture, and molecular biology

Reagents were purchased at the highest grade available. Ru360 was synthesized in-house following a previously published protocol (*Ying et al., 1991*). Genes encoding uniporter subunits were cloned into a pcDNA 3.1 (+) expression vector. Site-directed mutagenesis was performed using a QuickChange kit (Agilent) and confirmed with sequencing. All MCU constructs used here contain a C-terminal 1D4 tag (TETSQVAPA) for Western detection. Similarly, MICU1 is tagged with a C-terminal FLAG (DYKDDDDK), and MICU2 with a C-terminal FLAG or V5 (GKPIPNPLLGLDST). Sequences of these have been reported in a previous manuscript (*Tsai et al., 2016*).

HEK 293 cells, obtained from ATCC and authenticated by short tandem repeat profiling, were cultured in Dulbecco's modified Eagle's medium (Gibco) supplemented with 10% FBS, and were incubated at 37˚C with 5% CO_2. Mycoplasma infection was routinely ruled out using an ATCC PCR detection kit (30–1012K). CRISPR knockout cell lines have been established in our previous work (*Tsai et al., 2016*; *Tsai et al., 2017*). Transient transfection was performed using Lipofectamine 3000 (ThermoFisher), following the manufacturer's instructions. Cells were harvested for experiments 24–30 hr after transfection.

Co-immunoprecipitation (CoIP)

All CoIP experiments were performed at 4˚C. Transfected cells in 2 wells of a 6-well plate were lysed in 0.5 mL solubilization buffer (SB, 100 mM NaCl, 20 mM Tris, 1 mM EGTA, 5 mM DDM, pH 7.5-HCl) supplemented with an EDTA-free protease inhibitor cocktail (cOmplete Ultra, Roche). The lysate was clarified by spinning down. 50 µL of the supernatant was removed, with total protein concentration determined using a BCA assay (Thermo-Fisher) and 10 µg of protein used for whole-cell lysate (WCL) analysis. Then, 25 µL of FLAG (Sigma-Aldrich, A2220)- or 1D4-conjugated beads (50% slurry) were added to the rest of the supernatant for a 30 min batch binding process. The beads were then collected on a spin column, washed with 2 mL of SB, and then eluted with 0.15 mL SDS loading buffer. 10–20 µL of the elute was used for SDS-PAGE, with 5% of 2-mercaptoethanol used to produce reducing conditions. The whole CoIP procedure was completed within 45 min after cell lysis (prolonged incubation of >2 hr could lead to complete dissociation of uniporter subcomplexes). 1D4-affinity gel was produced in house using 25 mg 1D4 antibody per 1 g of CNBr-activated Sepharose 4B resin (GE Healthcare).

To perform Western blot, proteins on SDS gels were transferred to low-fluoresce PVDF membranes (EMD-Millipore), which were then blocked in a TBS-based Odyssey blocking buffer (Li-Cor), and incubated with primary antibodies in TBST (TBS +0.075% Tween-20) at 4˚C overnight. Then, after a 1 hr incubation with infrared fluorescent secondary antibodies in TBST at room temperature, signals were acquired using an Odyssey CLx imaging system (Li-Cor), and analyzed with an Image-Studio software (Li-Cor version 5.0). Unless specified, MCU and MICU1 were detected using $\alpha-$1D4 and α-FLAG antibodies, respectively. See the key resources table for antibodies and dilutions. 1D4 and C8 antibodies were produced in house.

Mitochondrial Ca^{2+} flux assays

For the fluorescence-based assay, 2×10^7 HEK 293 cells were suspended in 10 mL of wash buffer (WB, 120 mM KCl, 25 mM HEPES, 2 mM KH_2PO_4, 1 mM $MgCl_2$, 50 µM EGTA, pH 7.2-KOH), pelleted, and then resuspended in 2.5 mL of recording buffer (RB, 120 mM KCl, 25 mM HEPES, 2 mM KH_2PO_4, 5 mM succinate, 1 mM $MgCl_2$, 5 µM thapsigargin pH 7.2-KOH). 2 mL of the cell suspension were placed in a stirred quartz cuvette in a Hitachi F-2500 spectrophotometer (ex: 506 nm, ex-slit: 2.5 nm, em: 532 nm, em-slit: 2.5 nm, sampling rate: 2 Hz). Reagents were added into the cell suspension in the following order: 0.5 µM calcium green 5N (Thermo-Fisher C3737), 30 µM digitonin (Sigma-Aldrich D141), 10 µM $CaCl_2$, and 75 nM Ru360. Upon adding Ca^{2+}, fluorescent signals would increase by 200 to 300 a.u. Without adding Ru360, the signal would eventually drop to a steady-state level roughly the same as that before Ca^{2+} addition. Quantification of data is done by linear fit to the fluorescent signal between 10 s and 15 s after adding Ca^{2+}.

For the $^{45}Ca^{2+}$ based assay, 1.2–2.4 * 10^6 viable cells were suspended in 1 mL WB, spun down, and then resuspended in 120 µL WB, supplemented with 5 µM thapsigargin (Sigma-Aldrich, T9033) and 30 µM digitonin. To initiate mitochondrial Ca^{2+} uptake, 100 µL cell suspension was transferred to 400 µL low-Ca^{2+} flux buffer (RB +0.69 mM EGTA, 0.5 mM $CaCl_2$, 15 µM $^{45}CaCl_2$, 30 µM digitonin,

5 μM thapsigargin, pH 7.2-KOH) or high-Ca^{2+} flux buffer (RB +20 μM $^{45}CaCl_2$, 30 μM digitonin, 5 μM thapsigargin, pH 7.2-KOH). At desired time points, Ca^{2+} uptake was terminated by adding 100 μL of the sample to 5 mL ice-cold WB, and then filtered through 0.45 μM nitrocellulose membranes (Sigma-Aldrich WHA10402506) on a vacuum filtration manifold (EMD-Millipore model 1225). The membrane was washed immediately with 5 mL ice-cold WB, and later transferred into scintillation vials for counting. Nonspecific signals were measured using samples containing 75 nM Ru360 or using untransfected cells (for the Ru360-insensitive D261A mutant), and were subtracted to yield uniporter-specific Ca^{2+} transport. In a typical experiment, readings of $^{45}Ca^{2+}$ in three time points were fit with a linear function to generate the rate of Ca^{2+} transport (*e.g.*, ***Figure 7A***). Rates obtained from at least three independent experiments were then averaged for data presentation (see ***Figure 7—figure supplement 1*** for examples of the data analysis process). For experiments comparing WT and D261A, 1 μg WT DNA or 2.2 μg D261A DNA was used for transfection to ensure similar expression levels of these two constructs. Moreover, cells were harvested within 24 hr after transfection to avoid a molecular excess of overexpressed MCU over native MICU1. $^{45}Ca^{2+}$ radioisotope was obtained from PerkinElmer, and has a specific activity of 12–15 mCi/mg.

Sequence analysis and statistics

Sequences of MICU1 homologues were collected using PSI-BLAST. Multiple sequence alignment was performed using the Clustal Omega online server (***Sievers et al., 2011***).

All experiments were repeated in at least three independent experiments, and the data were presented as mean ±standard error of the mean (SEM). Statistical analysis was performed using Student's t-test, with significance defined as $p<0.05$.

Acknowledgements

We thank Carole Williams for technical assistance in molecular biology, and Dr. Christopher Miller for critical reading of this manuscript as well as providing unconditional support during the development of this project. We thank Dr. Vamsi Mootha for kindly providing an independent strain of MICU1-KO cells for us to verify results in ***Figure 7***. CWT and MFT are partly supported by the NIH grant R01-GM129345. The authors declare no conflict of interests.

Additional information

Funding

Funder	Grant reference number	Author
National Institute of General Medical Sciences	R01-GM129345	Chen-Wei Tsai Ming-Feng Tsai

The funders had no role in study design, data collection and interpretation, or the decision to submit the work for publication. The funders pay for the authors' salary and other research expenses.

Author contributions

Charles B Phillips, Chen-Wei Tsai, Conceptualization, Data curation, Formal analysis, Validation, Investigation, Writing—review and editing; Ming-Feng Tsai, Conceptualization, Data curation, Formal analysis, Supervision, Funding acquisition, Validation, Investigation, Writing—original draft, Project administration, Writing—review and editing

Author ORCIDs

Ming-Feng Tsai https://orcid.org/0000-0003-4277-1885

Decision letter and Author response

Decision letter https://doi.org/10.7554/eLife.41112.025
Author response https://doi.org/10.7554/eLife.41112.026

Additional files

Supplementary files

- Transparent reporting form

DOI: https://doi.org/10.7554/eLife.41112.021

Data availability

All data generated or analyzed during this study are included in the manuscript and supporting files. Source data for calcium-45 flux experiments are available via Dryad.

The following dataset was generated:

Author(s)	Year	Dataset title	Dataset URL	Database and Identifier
Phillips C, Tsai C, Tsai M	2019	Date from: The conserved aspartate ring of MCU mediates MICU1 binding and regulation in the mitochondrial calcium uniporter complex	https://doi.org/10.5061/dryad.1976kg3	Dryad Digital Repository, 10.5061/dryad.1976kg3

References

Almers W, McCleskey EW, Palade PT. 1984. A non-selective cation conductance in frog muscle membrane blocked by micromolar external calcium ions. *The Journal of Physiology* **353**:565–583. DOI: https://doi.org/10.1113/jphysiol.1984.sp015351, PMID: 6090645

Arduino DM, Wettmarshausen J, Vais H, Navas-Navarro P, Cheng Y, Leimpek A, Ma Z, Delrio-Lorenzo A, Giordano A, Garcia-Perez C, Médard G, Kuster B, García-Sancho J, Mokranjac D, Foskett JK, Alonso MT, Perocchi F. 2017. Systematic identification of MCU modulators by orthogonal interspecies chemical screening. *Molecular Cell* **67**:711–723. DOI: https://doi.org/10.1016/j.molcel.2017.07.019, PMID: 28820965

Banerjee A, Lee A, Campbell E, Mackinnon R. 2013. Structure of a pore-blocking toxin in complex with a eukaryotic voltage-dependent K(+) channel. *eLife* **2**:e00594. DOI: https://doi.org/10.7554/eLife.00594, PMID: 23705070

Baradaran R, Wang C, Siliciano AF, Long SB. 2018. Cryo-EM structures of fungal and metazoan mitochondrial calcium uniporters. *Nature* **559**:580–584. DOI: https://doi.org/10.1038/s41586-018-0331-8, PMID: 29995857

Baughman JM, Perocchi F, Girgis HS, Plovanich M, Belcher-Timme CA, Sancak Y, Bao XR, Strittmatter L, Goldberger O, Bogorad RL, Koteliansky V, Mootha VK. 2011. Integrative genomics identifies MCU as an essential component of the mitochondrial calcium uniporter. *Nature* **476**:341–345. DOI: https://doi.org/10.1038/nature10234, PMID: 21685886

Bick AG, Calvo SE, Mootha VK. 2012. Evolutionary diversity of the mitochondrial calcium uniporter. *Science* **336**:886. DOI: https://doi.org/10.1126/science.1214977, PMID: 22605770

Bick AG, Wakimoto H, Kamer KJ, Sancak Y, Goldberger O, Axelsson A, DeLaughter DM, Gorham JM, Mootha VK, Seidman JG, Seidman CE. 2017. Cardiovascular homeostasis dependence on MICU2, a regulatory subunit of the mitochondrial calcium uniporter. *PNAS* **114**:E9096–E9104. DOI: https://doi.org/10.1073/pnas.1711303114, PMID: 29073106

Cao C, Wang S, Cui T, Su XC, Chou JJ. 2017. Ion and inhibitor binding of the double-ring ion selectivity filter of the mitochondrial calcium uniporter. *PNAS* **114**:E2846–E2851. DOI: https://doi.org/10.1073/pnas.1620316114, PMID: 28325874

Csordás G, Golenár T, Seifert EL, Kamer KJ, Sancak Y, Perocchi F, Moffat C, Weaver D, de la Fuente Perez S, Bogorad R, Koteliansky V, Adijanto J, Mootha VK, Hajnóczky G. 2013. MICU1 controls both the threshold and cooperative activation of the mitochondrial Ca^{2+} uniporter. *Cell Metabolism* **17**:976–987. DOI: https://doi.org/10.1016/j.cmet.2013.04.020, PMID: 23747253

De Stefani D, Raffaello A, Teardo E, Szabò I, Rizzuto R. 2011. A forty-kilodalton protein of the inner membrane is the mitochondrial calcium uniporter. *Nature* **476**:336–340. DOI: https://doi.org/10.1038/nature10230, PMID: 21685888

Fan C, Fan M, Orlando BJ, Fastman NM, Zhang J, Xu Y, Chambers MG, Xu X, Perry K, Liao M, Feng L. 2018. X-ray and cryo-EM structures of the mitochondrial calcium uniporter. *Nature* **559**:575–579. DOI: https://doi.org/10.1038/s41586-018-0330-9

Hess P, Tsien RW. 1984. Mechanism of ion permeation through calcium channels. *Nature* **309**:453–456. DOI: https://doi.org/10.1038/309453a0, PMID: 6328315

Kamer KJ, Grabarek Z, Mootha VK. 2017. High-affinity cooperative Ca^{2+} binding by MICU1-MICU2 serves as an on-off switch for the uniporter. *EMBO reports* **18**:1397–1411. DOI: https://doi.org/10.15252/embr.201643748, PMID: 28615291

Kamer KJ, Mootha VK. 2015. The molecular era of the mitochondrial calcium uniporter. *Nature Reviews Molecular Cell Biology* **16**:545–553. DOI: https://doi.org/10.1038/nrm4039, PMID: 26285678

Kirichok Y, Krapivinsky G, Clapham DE. 2004. The mitochondrial calcium uniporter is a highly selective ion channel. *Nature* **427**:360–364. DOI: https://doi.org/10.1038/nature02246, PMID: 14737170

Kovács-Bogdán E, Sancak Y, Kamer KJ, Plovanich M, Jambhekar A, Huber RJ, Myre MA, Blower MD, Mootha VK. 2014. Reconstitution of the mitochondrial calcium uniporter in yeast. *PNAS* **111**:8985–8990. DOI: https://doi.org/10.1073/pnas.1400514111, PMID: 24889638

Logan CV, Szabadkai G, Sharpe JA, Parry DA, Torelli S, Childs AM, Kriek M, Phadke R, Johnson CA, Roberts NY, Bonthron DT, Pysden KA, Whyte T, Munteanu I, Foley AR, Wheway G, Szymanska K, Natarajan S, Abdelhamed ZA, Morgan JE, et al. 2014. Loss-of-function mutations in MICU1 cause a brain and muscle disorder linked to primary alterations in mitochondrial calcium signaling. *Nature Genetics* **46**:188–193. DOI: https://doi.org/10.1038/ng.2851, PMID: 24336167

Mallilankaraman K, Doonan P, Cárdenas C, Chandramoorthy HC, Müller M, Miller R, Hoffman NE, Gandhirajan RK, Molgó J, Birnbaum MJ, Rothberg BS, Mak DO, Foskett JK, Madesh M. 2012. MICU1 is an essential gatekeeper for MCU-mediated mitochondrial Ca(2+) uptake that regulates cell survival. *Cell* **151**:630–644. DOI: https://doi.org/10.1016/j.cell.2012.10.011, PMID: 23101630

Matlib MA, Zhou Z, Knight S, Ahmed S, Choi KM, Krause-Bauer J, Phillips R, Altschuld R, Katsube Y, Sperelakis N, Bers DM. 1998. Oxygen-bridged dinuclear ruthenium amine complex specifically inhibits Ca2+ uptake into mitochondria in vitro and in situ in single cardiac myocytes. *The Journal of Biological Chemistry* **273**:10223–10231. PMID: 9553073

Nguyen NX, Armache J-P, Lee C, Yang Y, Zeng W, Mootha VK, Cheng Y, Bai X-chen, Jiang Y. 2018. Cryo-EM structure of a fungal mitochondrial calcium uniporter. *Nature* **559**:570–574. DOI: https://doi.org/10.1038/s41586-018-0333-6

Paillard M, Csordás G, Huang KT, Várnai P, Joseph SK, Hajnóczky G. 2018. MICU1 interacts with the D-Ring of the MCU pore to control its Ca^{2+} Flux and Sensitivity to Ru360. *Molecular Cell* **72**:778–785. DOI: https://doi.org/10.1016/j.molcel.2018.09.008, PMID: 30454562

Park CS, Miller C. 1992. Interaction of charybdotoxin with permeant ions inside the pore of a K+ channel. *Neuron* **9**:307–313. DOI: https://doi.org/10.1016/0896-6273(92)90169-E, PMID: 1379820

Patron M, Checchetto V, Raffaello A, Teardo E, Vecellio Reane D, Mantoan M, Granatiero V, Szabò I, De Stefani D, Rizzuto R. 2014. MICU1 and MICU2 finely tune the mitochondrial Ca2+ uniporter by exerting opposite effects on MCU activity. *Molecular Cell* **53**:726–737. DOI: https://doi.org/10.1016/j.molcel.2014.01.013, PMID: 24560927

Payne R, Hoff H, Roskowski A, Foskett JK. 2017. MICU2 restricts spatial crosstalk between $InsP_3R$ and MCU channels by regulating threshold and gain of MICU1-Mediated inhibition and activation of MCU. *Cell Reports* **21**:3141–3154. DOI: https://doi.org/10.1016/j.celrep.2017.11.064, PMID: 29241542

Perocchi F, Gohil VM, Girgis HS, Bao XR, McCombs JE, Palmer AE, Mootha VK. 2010. MICU1 encodes a mitochondrial EF hand protein required for Ca(2+) uptake. *Nature* **467**:291–296. DOI: https://doi.org/10.1038/nature09358, PMID: 20693986

Petrungaro C, Zimmermann KM, Küttner V, Fischer M, Dengjel J, Bogeski I, Riemer J. 2015. The ca(2+)-Dependent release of the Mia40-Induced MICU1-MICU2 dimer from MCU regulates mitochondrial ca(2+) Uptake. *Cell Metabolism* **22**:721–733. DOI: https://doi.org/10.1016/j.cmet.2015.08.019, PMID: 26387864

Plovanich M, Bogorad RL, Sancak Y, Kamer KJ, Strittmatter L, Li AA, Girgis HS, Kuchimanchi S, De Groot J, Speciner L, Taneja N, Oshea J, Koteliansky V, Mootha VK. 2013. MICU2, a paralog of MICU1, resides within the mitochondrial uniporter complex to regulate calcium handling. *PLOS ONE* **8**:e55785. DOI: https://doi.org/10.1371/journal.pone.0055785, PMID: 23409044

Rizzuto R, De Stefani D, Raffaello A, Mammucari C. 2012. Mitochondria as sensors and regulators of calcium signalling. *Nature Reviews Molecular Cell Biology* **13**:566–578. DOI: https://doi.org/10.1038/nrm3412, PMID: 22850819

Sancak Y, Markhard AL, Kitami T, Kovács-Bogdán E, Kamer KJ, Udeshi ND, Carr SA, Chaudhuri D, Clapham DE, Li AA, Calvo SE, Goldberger O, Mootha VK. 2013. EMRE is an essential component of the mitochondrial calcium uniporter complex. *Science* **342**:1379–1382. DOI: https://doi.org/10.1126/science.1242993, PMID: 24231807

Shamseldin HE, Alasmari A, Salih MA, Samman MM, Mian SA, Alshidi T, Ibrahim N, Hashem M, Faqeih E, Al-Mohanna F, Alkuraya FS. 2017. A null mutation in MICU2 causes abnormal mitochondrial calcium homeostasis and a severe neurodevelopmental disorder. *Brain* **140**:2806–2813. DOI: https://doi.org/10.1093/brain/awx237, PMID: 29053821

Sievers F, Wilm A, Dineen D, Gibson TJ, Karplus K, Li W, Lopez R, McWilliam H, Remmert M, Söding J, Thompson JD, Higgins DG. 2011. Fast, scalable generation of high-quality protein multiple sequence alignments using clustal omega. *Molecular Systems Biology* **7**:539. DOI: https://doi.org/10.1038/msb.2011.75, PMID: 21988835

Tsai MF, Phillips CB, Ranaghan M, Tsai CW, Wu Y, Willliams C, Miller C. 2016. Dual functions of a small regulatory subunit in the mitochondrial calcium uniporter complex. *eLife* **5**:e15545. DOI: https://doi.org/10.7554/eLife.15545, PMID: 27099988

Tsai CW, Wu Y, Pao PC, Phillips CB, Williams C, Miller C, Ranaghan M, Tsai MF. 2017. Proteolytic control of the mitochondrial calcium uniporter complex. *PNAS* **114**:4388–4393. DOI: https://doi.org/10.1073/pnas.1702938114, PMID: 28396416

Tsai CW, Tsai MF. 2018. Electrical recordings of the mitochondrial calcium uniporter in *xenopus* oocytes. *The Journal of General Physiology* **150**. DOI: https://doi.org/10.1085/jgp.201812015, PMID: 29891485

Wang L, Yang X, Li S, Wang Z, Liu Y, Feng J, Zhu Y, Shen Y. 2014. Structural and mechanistic insights into MICU1 regulation of mitochondrial calcium uptake. *The EMBO Journal* **33**:594–604. DOI: https://doi.org/10.1002/embj.201386523, PMID: 24514027

Ying WL, Emerson J, Clarke MJ, Sanadi DR. 1991. Inhibition of mitochondrial calcium ion transport by an oxo-bridged dinuclear ruthenium ammine complex. *Biochemistry* **30**:4949–4952. PMID: 2036363

Yoo J, Wu M, Yin Y, Herzik MA, Lander GC, Lee S-Y. 2018. Cryo-EM structure of a mitochondrial calcium uniporter. *Science*:eaar4056. DOI: https://doi.org/10.1126/science.aar4056